Steel and Composite Structures, *Vol. 35, No. 4 (2020) 567-578*
DOI: https://doi.org/10.12989/scs.2020.35.4.567

Post-buckling of higher-order stiffened metal foam curved shells with porosity distributions and geometrical imperfection

Seyed Sajad Mirjavadi[1], Masoud Forsat*[1], Mohammad Reza Barati[2] and A.M.S. Hamouda[1]

[1]*Department of Mechanical and Industrial Engineering, Qatar University, P.O. Box 2713, Doha, Qatar*
[2]*Fidar project Qaem Company, Darvazeh Dolat, Tehran, Iran*

(*Received February 3, 2020, Revised April 20, 2020, Accepted April 30, 2020*)

Abstract. Based on third-order shear deformation shell theory, the present paper investigates post-buckling properties of eccentrically stiffened metal foam curved shells/panels having initial geometric imperfectness. Metal foam is considered as porous material with uniform and non-uniform models. The single-curve porous shell is subjected to in-plane compressive loads leading to post-critical stability in nonlinear regime. Via an analytical trend and employing Airy stress function, the nonlinear governing equations have been solved for calculating the post-buckling loads of stiffened geometrically imperfect metal foam curved shell. New findings display the emphasis of porosity distributions, geometrical imperfectness, foundation factors, stiffeners and geometrical parameters on post-buckling properties of porous curved shells/panels.

Keywords: post-buckling; shell theory; porous material; curved shell; third-order theory

1. Introduction

Metal foams are in the category of porous materials with low weight due to possessing different variations of porosities in them (Ahmed *et al*. 2019, Al-Maliki *et al*. 2019). Applying mechanical loads to such material structures yields elastic deformations and changed vibrational properties. The variation of porosities in this material causes a significant difference between metal foams and other perfect metals. In a non-perfect metal, the material characteristics are notably influenced by pore variations. Also, this variation in pores can affect the vibration frequencies of engineering structures made of metal foams. This issue can be understood from the works done by Chen *et al*. 2015, 2016. Different from metal foams, there are also functionally graded (FG) or ceramic-metal materials in which pore variation effect is very important (Abdelaziz *et al.* 2017, Zarga *et al*. 2019, Zine *et al.* 2018, Medani *et al*. 2019, Meksi *et al*. 2019, Mahmoudi *et al*. 2019, Draiche *et al.* 2019, Alimirzaei *et al.* 2019, Karami *et al.* 2019, Tlidji *et al.* 2019, Kaddari *et al*. 2020). In this material, pores may be produced in a phase between ceramic and material (Attia *et al*. 2018, Addou *et al*. 2019). Engineering structures made of this materials are studied to understand their vibration behaviors as reported in the works of Wattanasakulpong *et al.* (2014), Atmane *et al.* 2015). This type of material is used in different structures such as beams, plates and shells (Bellifa *et al.* 2017, Boukhlif *et al.* 2019). There are some studies on different structures in the literature (Nebab *et al.* 2019, Mirjavadi *et al*. 2017, 2018, 2019, Azimi *et al.* 2017, 2018).

Curved shell structures with single or double curvatures have been placed in the category of modern structural elements, mostly employed in some industrial applications including space vehicles, aircrafts, ocean constructions and in other substantial industrial fields. The investigation of static and dynamic behaviors of such structures is vital for having an efficient and dependable design (Kim *et al.* 2019, Quan *et al.* 2019). Recently, some authors studied mechanical behaviors of curved shells made of different materials (Trinh and Kim 2018, 2019a). Zare Jouneghani *et al.* (2017) examined linear vibration properties of FG double-curve shells based on porosity effects. Zhao et al. (2019) examined linear vibrations of porous FG shells with considering general types of boundary conditions. Also, Li *et al.* (2019) provided a numerical solution for free vibrations of FG shells with double curvatures and non-uniform thickness. Trinh *et al.* (2019) explored the temperature and porosity impacts on free vibration characteristics of FG double-curve shells. Most recently Trinh and Kim (2019b) presented a three-variable formulation for studying porous doubly-curved shells.

All of above mentioned articles related to porous curved shells neglects the influences of geometrical imperfection and stiffeners. Geometry imperfections are created during operation life or set up of curved shells and result in changed mechanical properties (Barati and Zenkour 2018). Plates/shells having stiffeners have been classified as reinforced structures with enhanced load bearing capacity, and are extensively employed in novel industrial fields. Thus, there have been many studies on the stability and dynamics of stiffened structures (Duc *et al*. 2016). Based on above discussion, nonlinear stability analysis of geometrically imperfect and stiffened curved porous shells under mechanical loads is not performed yet.

*Corresponding author, Professor
E-mail: masoudforsatlar@gmail.com

http://www.techno-press.org/?journal=scs&subpage=8
ISSN: 1229-9367 (Print), 1598-6233 (Online)

Based on third-order shear deformation shell theory, the present paper investigates post-buckling properties of eccentrically stiffened metal foam curved shells/panels having initial geometric imperfectness. Metal foam is considered as porous material with uniform and non-uniform models. The single-curve porous shell is subjected to in-plane compressive loads leading to post-critical stability in nonlinear regime. Via an analytical trend and employing Airy stress function, the nonlinear governing equations have been solved for calculating the post-buckling loads of stiffened geometrically imperfect metal foam curved shell. New findings display the emphasis of porosity distributions, geometrical imperfectness, foundation factors, stiffeners and geometrical parameters on post-buckling properties of porous curved shells/panels.

A porous material, for instance a steel foam, might be placed in the category of lightweight materials and can be applied in several structures such as curved panels. Often, pore variation along the thickness of shells results in a notable alteration in every kind of material property. When the pore distribution inside the material is selected to be non-uniform, the metal foam might be defined as a functionally graded material since its properties obey some specified functions. Herein, the following types of pore dispersion will be employed (Ahmed *et al.* 2019, Fenjan *et al.* 2019)

- Uniform kind

$$E = E_2(1-e_0\chi) \tag{1a}$$

$$G = G_2(1-e_0\chi) \tag{1b}$$

$$\rho = \rho_2\sqrt{(1-e_0\chi)} \tag{1c}$$

- Non-uniform kind

$$E(z) = E_2(1-e_0\cos\left(\frac{\pi z}{h}\right)) \tag{2a}$$

$$G(z) = G_2(1-e_0\cos\left(\frac{\pi z}{h}\right)) \tag{2b}$$

$$\rho(z) = \rho_2(1-e_m\cos\left(\frac{\pi z}{h}\right)) \tag{2c}$$

The most important factors in above relations are the main values of material properties E_2, G_2 and ρ_2. Also, there are two important factors related to pores and mass which are e_0 and e_m as

$$e_0 = 1-\frac{E_2}{E_1} = 1-\frac{G_2}{G_1}, e_m = 1-\frac{\rho_2}{\rho_1} = 1-\sqrt{1-e_0} \tag{3}$$

In above relations properties E_1, G_1 and ρ_1 denote the material properties at top/bottom surfaces of the shell. Based on the open cell assumption of porous material, we use the following relations

$$\frac{E_2}{E_1} = \left(\frac{\rho_2}{\rho_1}\right)^2 \tag{4}$$

Based on uniformly distributed pores, the following parameter is used in Eq. (1) as (Ahmed *et al.* 2019)

$$\chi = \frac{1}{e_0} - \frac{1}{e_0}\left(\frac{2}{\pi}\sqrt{1-e_0} - \frac{2}{\pi} + 1\right)^2 \tag{5}$$

3. Governing equations

In this article, third-order shell theory has been employed for mathematical modeling of the curved shells. Thus, the strain field can be introduced by (Duc and Quan 2014, Zaoui *et al.* 2019)

$$\begin{Bmatrix} \varepsilon_x \\ \varepsilon_y \\ \gamma_{xy} \end{Bmatrix} = \begin{Bmatrix} \varepsilon_x^0 \\ \varepsilon_y^0 \\ \gamma_{xy}^0 \end{Bmatrix} + z\begin{Bmatrix} k_x \\ k_y \\ k_{xy} \end{Bmatrix} + z^3\begin{Bmatrix} \Upsilon_x \\ \Upsilon_y \\ \Upsilon_{xy} \end{Bmatrix}$$
$$\begin{Bmatrix} \gamma_{xz} \\ \gamma_{zy} \end{Bmatrix} = \begin{Bmatrix} \gamma_{xz}^0 \\ \gamma_{yz}^0 \end{Bmatrix} + z^2\begin{Bmatrix} k_{xz} \\ k_{zy} \end{Bmatrix} \tag{6}$$

in which

$$\begin{gathered}
\varepsilon_x^0 = \frac{\partial u}{\partial x} + \frac{1}{2}(\frac{\partial w}{\partial x})^2,\ \varepsilon_y^0 = \frac{\partial v}{\partial y} + \frac{1}{2}(\frac{\partial w}{\partial y})^2 - \frac{w}{R}, \\
\gamma_{xy}^0 = \frac{\partial u}{\partial y} + \frac{\partial v}{\partial x} + \frac{\partial w}{\partial x}\frac{\partial w}{\partial y}, \\
\gamma_{xz}^0 = \varphi_x + \frac{\partial w}{\partial x}, \gamma_{yz}^0 = \varphi_y + \frac{\partial w}{\partial y}, \\
k_x = \frac{\partial \varphi_x}{\partial x},\ k_y = \frac{\partial \varphi_y}{\partial y},\ k_{xy} = \frac{\partial \varphi_x}{\partial y} + \frac{\partial \varphi_y}{\partial x} \\
\Upsilon_x = -c_1(\frac{\partial \varphi_x}{\partial x} + \frac{\partial^2 w}{\partial x^2}), \\
\Upsilon_y = -c_1(\frac{\partial \varphi_y}{\partial y} + \frac{\partial^2 w}{\partial y^2}) \\
\Upsilon_{xy} = -c_1(\frac{\partial \varphi_x}{\partial y} + \frac{\partial \varphi_y}{\partial x} + 2\frac{\partial^2 w}{\partial x \partial y}) \\
k_{xz} = -3c_1(\varphi_x + \frac{\partial w}{\partial x}) \\
k_{yz} = -3c_1(\varphi_y + \frac{\partial w}{\partial y})
\end{gathered} \tag{7}$$

where $c_1 = 4/3h^2$. The presented field contains transverse (w) and in-plane (u, v) components. Based on the higher-order shell assumption, stress-strain relations can be summarized as (Boulefrakh *et al.* 2019, Abualnour *et al.* 2019, Addou *et al.* 2019, Balubaid *et al*. 2019, Bedia *et al.* 2019, Belbachir *et al.* 2019, Berghouti *et al*. 2019, Bourada *et al.* 2019, Boutaleb *et al.* 2019, Chaabane *et al.* 2019, Khiloun *et al.* 2019, Hussain *et al.* 2019, Sahla *et al.* 2019)

$$\begin{Bmatrix} \sigma_x \\ \sigma_y \\ \sigma_{xy} \\ \sigma_{xz} \\ \sigma_{yz} \end{Bmatrix} = \begin{pmatrix} Q_{11} & Q_{12} & 0 & 0 & 0 \\ Q_{12} & Q_{22} & 0 & 0 & 0 \\ 0 & 0 & Q_{66} & 0 & 0 \\ 0 & 0 & 0 & Q_{44} & 0 \\ 0 & 0 & 0 & 0 & Q_{55} \end{pmatrix} \begin{Bmatrix} \varepsilon_x \\ \varepsilon_y \\ \gamma_{xy} \\ \gamma_{xz} \\ \gamma_{yz} \end{Bmatrix} \tag{8}$$
$$Q_{11} = Q_{22} = \frac{E(z)}{1-\upsilon^2},\ Q_{12} = \upsilon Q_{11},\ Q_{44} = Q_{55} = Q_{66} = \frac{E(z)}{2(1+\upsilon)}$$

where σ_i (i=x, y, xy) are stress field components. The stresses leads to below resultants via integrating Eq. (8) over shell thickness as

$$N_x = B_{11}\varepsilon_x^0 + B_{12}\varepsilon_y^0 + B_{13}k_x + B_{14}k_y + B_{15}\Upsilon_x + B_{16}\Upsilon_y \tag{9}$$

$$N_y = B_{12}\varepsilon_x^0 + B_{22}\varepsilon_y^0 + B_{14}k_x + B_{24}k_y + B_{16}\Upsilon_x + B_{26}\Upsilon_y \tag{10}$$

$$N_{xy} = B_{31}\gamma_{xy}^0 + B_{32}k_{xy} + B_{33}\Upsilon_{xy} \tag{11}$$

$$M_x = B_{13}\varepsilon_x^0 + B_{14}\varepsilon_y^0 + B_{43}k_x + B_{44}k_y + B_{45}\Upsilon_x + B_{46}\Upsilon_y \tag{12}$$

$$M_y = B_{14}\varepsilon_x^0 + B_{24}\varepsilon_y^0 + B_{44}k_x + B_{54}k_y + B_{46}\Upsilon_x + B_{56}\Upsilon_y \tag{13}$$

$$M_{xy} = B_{32}\gamma_{xy}^0 + B_{62}k_{xy} + B_{63}\Upsilon_{xy} \tag{14}$$

$$R_x = B_{71}\varepsilon_x^0 + B_{16}\varepsilon_y^0 + B_{73}k_x + B_{46}k_y + B_{75}\Upsilon_x + B_{76}\Upsilon_y \tag{15}$$

$$R_y = B_{16}\varepsilon_x^0 + B_{82}\varepsilon_y^0 + B_{46}k_x + B_{84}k_y + B_{76}\Upsilon_x + B_{86}\Upsilon_y \tag{16}$$

$$R_{xy} = B_{33}\gamma_{xy}^0 + B_{63}k_{xy} + B_{93}\Upsilon_{xy} \tag{17}$$

$$Q_x = B_{94}\gamma_{xz}^0 + B_{95}k_{xz}, Q_y = B_{96}\gamma_{yz}^0 + B_{97}k_{yz}, \tag{18}$$

$$K_x = B_{98}\gamma_{xz}^0 + B_{99}k_{xz}, K_y = B_{100}\gamma_{yz}^0 + B_{101}k_{yz}. \tag{19}$$

in which

$$\begin{aligned}
&B_{11} = \int_{-h/2}^{h/2} Q_{11}dz + \frac{E_s A_{sx}}{s_x},\ B_{12} = \int_{-h/2}^{h/2} Q_{12}dz,\\
&B_{13} = \int_{-h/2}^{h/2} Q_{11}zdz + \frac{E_s A_{sx} z_x}{s_x}\\
&B_{14} = \int_{-h/2}^{h/2} Q_{12}zdz, B_{16} = \int_{-h/2}^{h/2} Q_{12}z^3dz,\\
&B_{15} = \int_{-h/2}^{h/2} Q_{11}z^3dz + \frac{E_s A_{sx}\left(z_x\right)^3}{s_x} + \frac{d_x\left(h_x\right)^3 E_s z_x}{4s_x},\\
&B_{22} = \int_{-h/2}^{h/2} Q_{22}dz + \frac{E_s A_{sy}}{s_y},\\
&B_{24} = \int_{-h/2}^{h/2} Q_{22}zdz + \frac{E_s A_{sy} z_y}{s_y},\\
&B_{26} = \int_{-h/2}^{h/2} Q_{22}z^3dz + \frac{E_s A_{sy}\left(z_y\right)^3}{s_y} + \frac{d_y\left(h_y\right)^3 E_s z_y}{4s_y},\\
&\{B_{31}, B_{32}, B_{33}\} = \int_{-h/2}^{h/2} Q_{66}\{1, z, z^3\}dz,\\
&B_{43} = \int_{-h/2}^{h/2} Q_{11}z^2dz + \frac{E_s A_{sx}\left(z_x\right)^2}{s_x} + \frac{d_x\left(h_x\right)^3 E_s}{12s_x},\\
&\{B_{44}, B_{46}, B_{76}\} = \int_{-h/2}^{h/2} Q_{12}\{z^2, z^4, z^6\}dz,\\
&B_{45} = \int_{-h/2}^{h/2} Q_{11}z^4dz + \frac{E_s A_{sx}\left(z_x\right)^4}{s_x} + \frac{d_x\left(h_x\right)^5 E_s}{80s_x} + \frac{d_x\left(h_x\right)^3\left(z_x\right)^2 E_s}{2s_x},\\
&B_{54} = \int_{-h/2}^{h/2} Q_{22}z^2dz + \frac{E_s A_{sy}\left(z_y\right)^2}{s_y} + \frac{d_y\left(h_y\right)^3 E_s}{12s_y},\\
&B_{56} = \int_{-h/2}^{h/2} Q_{22}z^4dz + \frac{E_s A_{sy}\left(z_y\right)^4}{s_y} + \frac{d_y\left(h_y\right)^5 E_s}{80s_y} + \frac{d_y\left(h_y\right)^3\left(z_y\right)^2 E_s}{2s_y},\\
&\{B_{62}, B_{63}, B_{93}\} = \int_{-h/2}^{h/2} Q_{66}\{z^2, z^4, z^6\}dz,\\
&B_{71} = \int_{-h/2}^{h/2} Q_{11}z^3dz + E_s A_{sx}\left(z_x\right)^3 + \frac{d_x\left(h_x\right)^3 E_s z_x}{4},\\
&B_{73} = \int_{-h/2}^{h/2} Q_{11}z^4dz + E_s A_{sx}\left(z_x\right)^4 + \frac{d_x\left(h_x\right)^5 E_s}{80} + \frac{d_x\left(h_x\right)^3\left(z_x\right)^2 E_s}{2},\\
&B_{82} = \int_{-h/2}^{h/2} Q_{22}z^3dz + E_s A_{sy}\left(z_y\right)^3 + \frac{d_y\left(h_y\right)^3 E_s z_y}{4},\\
&\{B_{94}, B_{95}, B_{99}\} = \int_{-h/2}^{h/2} Q_{44}\{1, z^2, z^4\}dz,\\
&\{B_{96}, B_{100}, B_{101}\} = \int_{-h/2}^{h/2} Q_{55}\{1, z^2, z^4\}dz,
\end{aligned} \tag{20}$$

where E_s is Young's modulus of stiffeners; s_x nd s_y are spacing of longitudinal and lateral stiffeners; A_{sx} and A_{sy} are cross sections of stiffeners and

$$z_x = 0.5(h + h_x), \quad z_y = 0.5(h + h_y) \tag{21}$$

Note that h_x and h_y are height of stiffeners; d_x and d_y are width of stiffeners. The well-known governing equations for a single-curved shells may be expressed by (Duc and Quan 2014)

$$\frac{\partial N_x}{\partial x} + \frac{\partial N_{xy}}{\partial y} = 0 \tag{22}$$

$$\frac{\partial N_{xy}}{\partial x} + \frac{\partial N_y}{\partial y} = 0 \tag{23}$$

$$\begin{aligned}
&\frac{\partial Q_x}{\partial x} + \frac{\partial Q_y}{\partial y} - 3c_1\left(\frac{\partial K_x}{\partial x} + \frac{\partial K_y}{\partial y}\right) + c_1\left(\frac{\partial^2 R_x}{\partial x^2} + 2\frac{\partial^2 R_{xy}}{\partial x \partial y} + \frac{\partial^2 R_y}{\partial y^2}\right) + \frac{N_y}{R}\\
&+ N_x\frac{\partial^2 w}{\partial x^2} + 2N_{xy}\frac{\partial^2 w}{\partial x \partial y} + N_y\frac{\partial^2 w}{\partial y^2} - k_w w + k_P\left(\frac{\partial^2 w}{\partial x^2} + \frac{\partial^2 w}{\partial y^2}\right) = 0
\end{aligned} \tag{24}$$

$$\frac{\partial M_x}{\partial x} + \frac{\partial M_{xy}}{\partial y} - Q_x + 3c_1 K_x - c_1\left(\frac{\partial R_x}{\partial x} + \frac{\partial R_{xy}}{\partial y}\right) = 0 \tag{25}$$

$$\frac{\partial M_y}{\partial y} + \frac{\partial M_{xy}}{\partial x} - Q_y + 3c_1 K_y - c_1\left(\frac{\partial R_y}{\partial y} + \frac{\partial R_{xy}}{\partial x}\right) = 0 \tag{26}$$

in which k_W and k_p are linear and shear foundation parameters. Now, using Eqs. (9)-(19), it is feasible to achieve three strains based on below relations

$$\begin{aligned}
&\varepsilon_x^0 = \frac{B_{22}}{B_{11}B_{12} - B_{12}^2}N_x - \frac{B_{12}}{B_{11}B_{12} - B_{12}^2}N_y - \frac{B_{13}B_{22} - B_{14}B_{12}}{B_{11}B_{12} - B_{12}^2}k_x\\
&- \frac{B_{14}B_{22} - B_{24}B_{12}}{B_{11}B_{12} - B_{12}^2}k_y - \frac{B_{15}B_{22} - B_{16}B_{12}}{B_{11}B_{12} - B_{12}^2}\Upsilon_x - \frac{B_{16}B_{22} - B_{26}B_{12}}{B_{11}B_{12} - B_{12}^2}\Upsilon_y,\\
&\varepsilon_y^0 = \frac{B_{11}}{B_{11}B_{12} - B_{12}^2}N_y - \frac{B_{12}}{B_{11}B_{12} - B_{12}^2}N_x - \frac{B_{11}B_{14} - B_{13}B_{12}}{B_{11}B_{12} - B_{12}^2}k_x\\
&- \frac{B_{11}B_{24} - B_{14}B_{12}}{B_{11}B_{12} - B_{12}^2}k_y - \frac{B_{11}B_{16} - B_{15}B_{12}}{B_{11}B_{12} - B_{12}^2}\Upsilon_x - \frac{B_{11}B_{26} - B_{16}B_{12}}{B_{11}B_{12} - B_{12}^2}\Upsilon_y,\\
&\gamma_{xy}^0 = -\frac{1}{B_{13}}N_{xy} - \frac{B_{32}}{B_{31}}k_{xy} - \frac{B_{33}}{B_{31}}\Upsilon_{xy}.
\end{aligned} \tag{27}$$

Now, the Airy stress function (F) can be introduced by (Chikh *et al.* 2016)

$$\frac{\partial^2 F}{\partial y^2} = N_x,\ \frac{\partial^2 F}{\partial x \partial y} = -N_{xy},\ \frac{\partial^2 F}{\partial x^2} = N_y \tag{28}$$

The specific compatibility relation of a single-curve shell taking into account geometric imperfectness might be written as (Duc and Quan 2014)

$$\begin{aligned}
&\frac{\partial^2 \varepsilon_x^0}{\partial y^2} + \frac{\partial^2 \varepsilon_y^0}{\partial x^2} - \frac{\partial^2 \gamma_{xy}^0}{\partial x \partial y} = \left(\frac{\partial^2 w}{\partial x \partial y}\right)^2 - \frac{\partial^2 w}{\partial x^2}\frac{\partial^2 w}{\partial y^2} + 2\frac{\partial^2 w}{\partial x \partial y}\frac{\partial^2 w^*}{\partial x \partial y} - \frac{\partial^2 w}{\partial x^2}\frac{\partial^2 w^*}{\partial y^2}\\
&- \frac{\partial^2 w}{\partial y^2}\frac{\partial^2 w^*}{\partial x^2} - \frac{1}{R}\frac{\partial^2 w}{\partial x^2}
\end{aligned} \tag{29}$$

Placing Eq. (27) in Eq. (29) results in the compatibility equation of an imperfect metal foam curved shell as

$$+J_1\frac{\partial^4 F}{\partial y^4}+J_2\frac{\partial^4 F}{\partial x^4}+J_3\frac{\partial^4 F}{\partial x^2\partial y^2}+J_4\frac{\partial^3\varphi_y}{\partial y^3}+J_5\frac{\partial^3\varphi_x}{\partial x\partial y^2}+J_6\frac{\partial^3\varphi_x}{\partial x^3}+J_7\frac{\partial^3\varphi_y}{\partial x^2\partial y}$$
$$+J_8\frac{\partial^4 w}{\partial x^4}+J_9\frac{\partial^4 w}{\partial y^4}+J_{10}\frac{\partial^4 w}{\partial x^2\partial y^2}=\left(\frac{\partial^2 w}{\partial x\partial y}\right)^2-\frac{\partial^2 w}{\partial x^2}\frac{\partial^2 w}{\partial y^2}+2\frac{\partial^2 w}{\partial x\partial y}\frac{\partial^2 w^*}{\partial x\partial y} \tag{30}$$
$$-\frac{\partial^2 w}{\partial x^2}\frac{\partial^2 w^*}{\partial y^2}-\frac{\partial^2 w}{\partial y^2}\frac{\partial^2 w^*}{\partial x^2}-\frac{1}{R}\frac{\partial^2 w}{\partial x^2}$$

where

$$J_1=\frac{B_{22}}{B_{11}B_{12}-B_{12}^2},\ J_2=\frac{B_{11}}{B_{11}B_{12}-B_{12}^2}$$
$$J_3=(\frac{1}{B_{13}}-2\frac{B_{12}}{B_{11}B_{12}-B_{12}^2})$$
$$J_4=c_1\frac{B_{16}B_{22}-B_{26}B_{12}}{B_{11}B_{12}-B_{12}^2}-\frac{B_{14}B_{22}-B_{24}B_{12}}{B_{11}B_{12}-B_{12}^2}$$
$$J_5=c_1\frac{B_{15}B_{22}-B_{16}B_{12}}{B_{11}B_{12}-B_{12}^2}-\frac{B_{13}B_{22}-B_{14}B_{12}}{B_{11}B_{12}-B_{12}^2}-c_1\frac{B_{33}}{B_{31}}+\frac{B_{32}}{B_{31}}$$
$$J_6=c_1\frac{B_{11}B_{16}-B_{15}B_{12}}{B_{11}B_{12}-B_{12}^2}-\frac{B_{11}B_{14}-B_{13}B_{12}}{B_{11}B_{12}-B_{12}^2} \tag{31}$$
$$J_7=c_1\frac{B_{11}B_{26}-B_{16}B_{12}}{B_{11}B_{12}-B_{12}^2}-\frac{B_{11}B_{14}-B_{14}B_{12}}{B_{11}B_{12}-B_{12}^2}-c_1\frac{B_{33}}{B_{31}}+\frac{B_{32}}{B_{31}}$$
$$J_8=c_1\frac{B_{11}B_{16}-B_{15}B_{12}}{B_{11}B_{12}-B_{12}^2}$$
$$J_9=c_1\frac{B_{16}B_{22}-B_{26}B_{12}}{B_{11}B_{12}-B_{12}^2}$$
$$J_{10}=c_1\frac{B_{11}B_{26}-B_{16}B_{12}}{B_{11}B_{12}-B_{12}^2}+c_1\frac{B_{15}B_{22}-B_{16}B_{12}}{B_{11}B_{12}-B_{12}^2}-c_1\frac{B_{33}}{B_{31}}$$

The post-buckling load of curved shell/panel may be calculated via solving Eqs. (24)-(26) and also Eq. (30).

4. Solution approach

Throughout the present chapter, the solution for the non-linear governing equations related to post-buckling of a metal foam curved shell has been introduced. In order to investigate the mechanical post-buckling of simply-supported shells, the freely moving boundary conditions become

$$w=\varphi_y=N_{xy}=M_x=R_x=0,\qquad \int_0^b N_x dy=-P_x h \quad \text{at } x=0,a \tag{32}$$

$$w=\varphi_x=N_{xy}=M_y=R_y=0,\qquad \int_0^a N_y dx=-P_y h \quad \text{at } y=0,b \tag{33}$$

Next, the displacement components take the below forms (Ahmed *et al*. 2019, Khosravi *et al*. 2020)

$$w=\sum_{m=1}^{\infty}\sum_{n=1}^{\infty}\tilde{W}\, f_m^w(x)g_n^w(y) \tag{34}$$

$$w^*=\sum_{m=1}^{\infty}\sum_{n=1}^{\infty}W^*\, f_m^{w*}(x)g_n^{w*}(y) \tag{35}$$

$$\varphi_x=\sum_{m=1}^{\infty}\sum_{n=1}^{\infty}\Phi_x\, f_m^{\varphi_x}(x)g_n^{\varphi_x}(y) \tag{36}$$

$$\varphi_y=\sum_{m=1}^{\infty}\sum_{n=1}^{\infty}\Phi_y\, f_m^{\varphi_y}(x)g_n^{\varphi_y}(y) \tag{37}$$

where $\tilde{W}$ and W^* define the deflection amplitudes and imperfectness amplitudes, respectively. For simply-supported edges let $f_m^w=f_m^{w*}=f_m^{\varphi_y}=\sin(\lambda_m x)$ with $\lambda_m=m\pi/a$ and $g_n^w=g_n^{w*}=g_n^{\varphi_x}=\sin(\delta_n y)$ with $\delta_n=n\pi/b$. In order to obtain stress function F, Eqs. (34)-(37) should be inserted into Eq. (30) together with satisfying boundary condition presented as Eqs. (32) and (33) which leads (Chikh *et al.* 2016)

$$F=\Phi_1\cos(2\lambda_m x)+\Phi_2\cos(2\delta_n y)+\Phi_3\sin(\lambda_m x)\sin(\delta_n y)+\frac{1}{2}P_x y^2+\frac{1}{2}P_y x^2 \tag{38}$$

where P_x and P_y are applied in-plane load in x and y directions and

$$\Phi_1=\frac{(B_{11}B_{12}-B_{12}^2)\delta_n^2}{32B_{11}\lambda_m^2}\tilde{W}(\tilde{W}+2W^*),$$
$$\Phi_1=\frac{(B_{11}B_{12}-B_{12}^2)\lambda_m^2}{32B_{22}\delta_n^2}\tilde{W}(\tilde{W}+2W^*),$$
$$\Phi_3=[\frac{1}{J_2\lambda_m^4+J_1\delta_n^4+J_3\lambda_m^2\delta_n^2}][-(J_5\lambda_m\delta_n^2+J_6\lambda_m^3)\Phi_x-(J_7\lambda_m^2\delta_n+J_4\delta_n^3)\Phi_y$$
$$-(J_8\lambda_m^4+J_9\delta_n^4+J_{10}\lambda_m^2\delta_n^2-\frac{\lambda_m^2}{R})\tilde{W}].$$

The governing equation can be reduced to the following form via inserting Eqs. (34)-(38) into Eqs. (24)-(26) and simply collecting the coefficients of $\tilde{W}$ and W^* by defining the coefficients as S_{ij}

$$S_{11}\tilde{W}+S_{21}\Phi_x+S_{31}\Phi_y+S_{41}(\tilde{W}+W^*)\Phi_x+S_{51}(\tilde{W}+W^*)\Phi_y$$
$$+n_1\tilde{W}(\tilde{W}+W^*)+n_2\tilde{W}(\tilde{W}+2W^*)+n_3\tilde{W}(\tilde{W}+W^*)(\tilde{W}+2W^*)=0 \tag{39}$$

$$S_{12}\tilde{W}+S_{22}\Phi_x+S_{32}\Phi_y+n_4\tilde{W}(\tilde{W}+W^*)+n_5\tilde{W}(\tilde{W}+2W^*)=0 \tag{40}$$

$$S_{13}\tilde{W}+S_{23}\Phi_x+S_{33}\Phi_y+n_6\tilde{W}(\tilde{W}+W^*)+n_7\tilde{W}(\tilde{W}+2W^*)=0 \tag{41}$$

where S_{ij} denote linear stiffness matrices and n_i denote nonlinear stiffness components. Herein, S_{ij} can be calculated by collecting the coefficients of $\tilde{W}$ and W^* and due to the reason that they have complex forms, it is not possible to express them in closed-form. Note that for studying nonlinear stability of single-curve shells under axial load (P_x), it is crucial to consider $P_y=0$. The nonlinear governing equation has been solved for finding post-buckling curves of the shell based on the variation of $P=P_x/(h*10^9)$ versus normalized deflection $\tilde{W}/h$. It must be stated that numerical investigations have been carried out based upon the following non-dimension definitions of the elastic foundation

$$K_W=\mathrm{k}_W\frac{\mathrm{a}^4}{D_{11}},\ K_p=\mathrm{k}_p\frac{\mathrm{a}^2}{D_{11}} \tag{42}$$

5. Discussions on findings

In this chapter, post-buckling of a porous single-curved shell modeled via nonlinear imperfect third-order shell

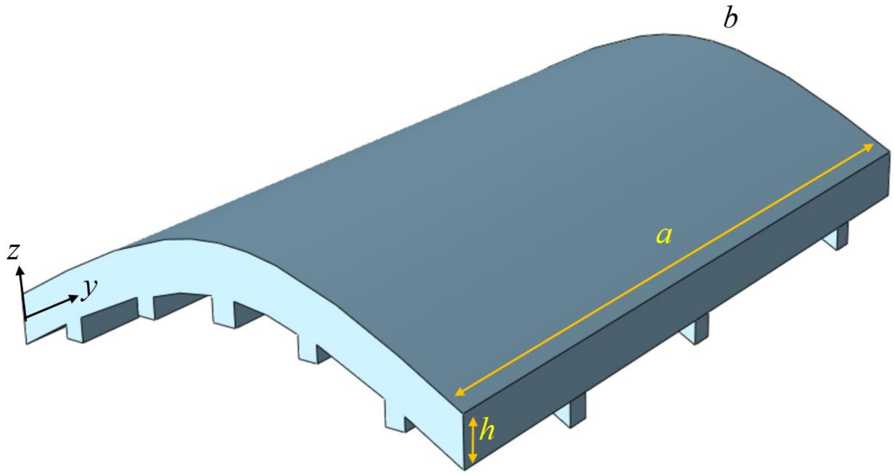

Fig. 1 Geometry of stiffened curved shells

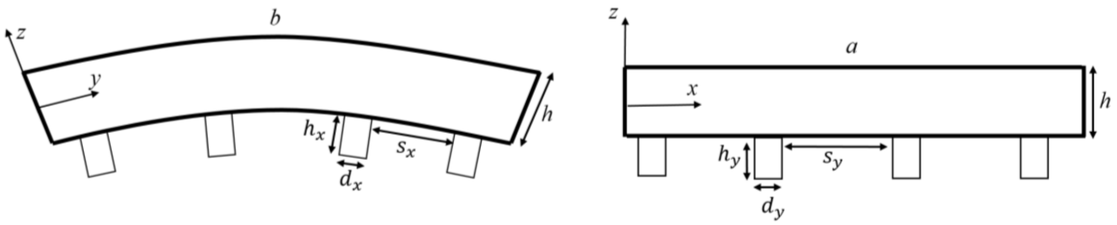

Fig. 2 Geometry and spacing of stiffeners

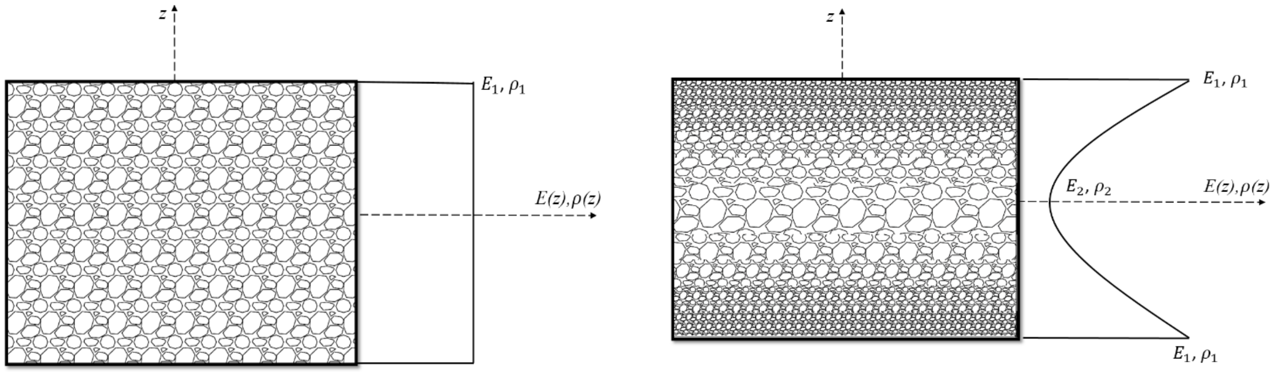

(a) Uniform (b) Non-uniform

Fig. 3 Two types of porosity distributions inside metal foam

theory gas been represented based upon offered solution approach. The single curved shell with stiffeners is shown in Figs.1 and 2. Also, porosity distributions are indicated in Fig.3. The adherence of non-linear buckling loads to the porosity distributions, foundation parameters, dimensionless amplitude, stiffeners, geometrical imperfection and geometrical factors will be discussed. As the first step, post-buckling behavior of ideal and imperfect flat panels (a/R_x=b/R_y=0) has been checked in comparison with those reported by Chikh *et al*. (2016) based on functionally graded (FG) flat panel model, as represented in Table 1. According to the table, buckling loads have been represented based upon both ideal ($W^*/h=0$) and imperfect ($W^*/h=0.1$) flat panel and diverse non-dimension amplitude. In this research, obtained results based on metal foam material are presented using the below properties:

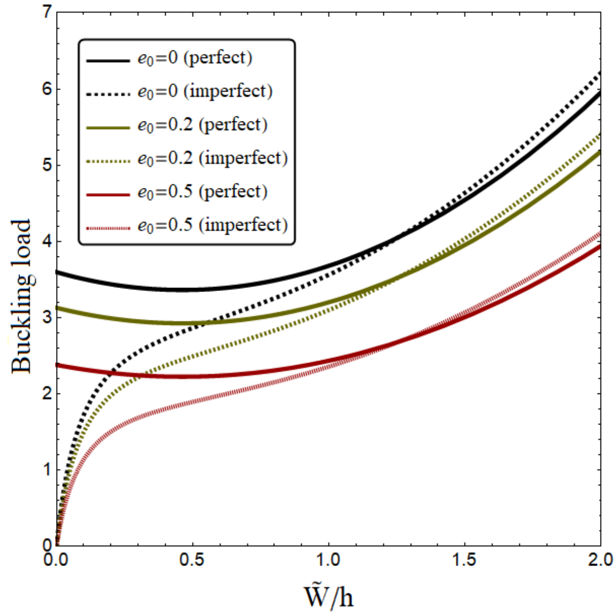

Fig. 4 Nonlinear buckling load versus normalized deflection of the shell for various porosity coefficients (a/h=15, R/a=4, W*/h=0.1)

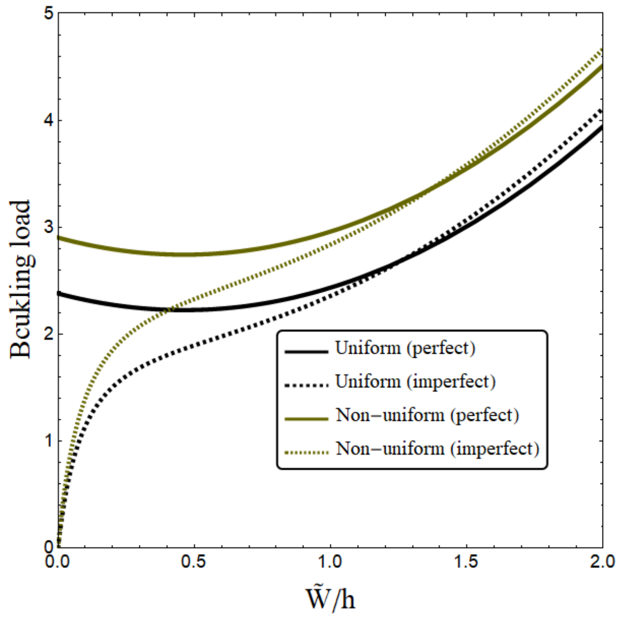

Fig. 5 Nonlinear buckling load versus normalized deflection of the shell for various porosity distributions (a/h=15, R/a=4, W*/h=0.1, e_0=0.5)

- $E_2 = 200\ GPa,\ \rho_2 = 7850\ kg/m^3,\ v = 0.33,$

Fig. 4 shows the influence of porosity coefficient on the post-buckling load of geometrically perfect and imperfect porous curved shells at *a/h*=50 and $W^*/h = 0.1$ for uniform porosity distribution. Various values of porosity coefficient are considered (e_0=0, 0.2 and 0.5). For an ideal (perfect) curved shell, the starting point ($\tilde{W}/h = 0$) is critical buckling load. But, for an imperfect doubly-curved shell ($W^*/h \neq 0$), there is no critical buckling load, since the shell is at its initial deflection. It is well-known that the nonlinear buckling load gets smaller with the increase of dimensionless amplitude. Then, it becomes larger with more increment in dimensionless amplitude. Actually, the post-buckling path of the single-curved shell is un-stable immediately after critical buckling. Also, increase of porosity coefficient results in smaller buckling loads for both ideal and imperfect curved shells. This is due to a

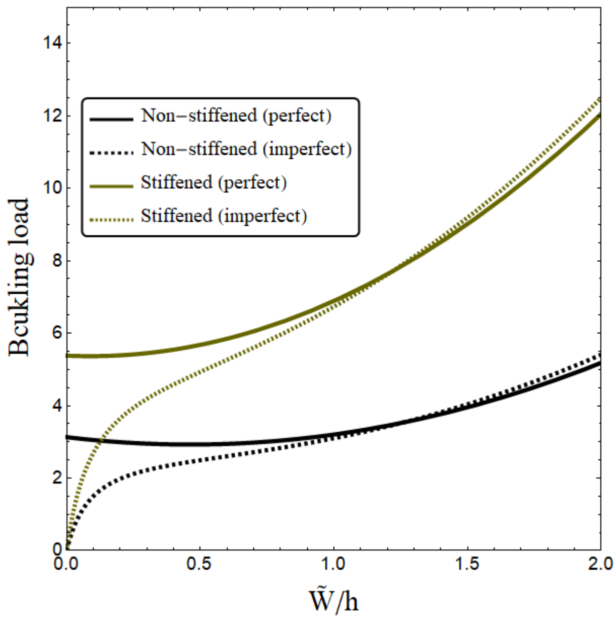

Fig. 6 Nonlinear buckling load versus normalized deflection of porous shell with and without stiffeners (a/h=15, R/a=4, W*/h=0.1, e_0=0.2, s_x=0.2a, h_x=0.1h, d_x=0.01a)

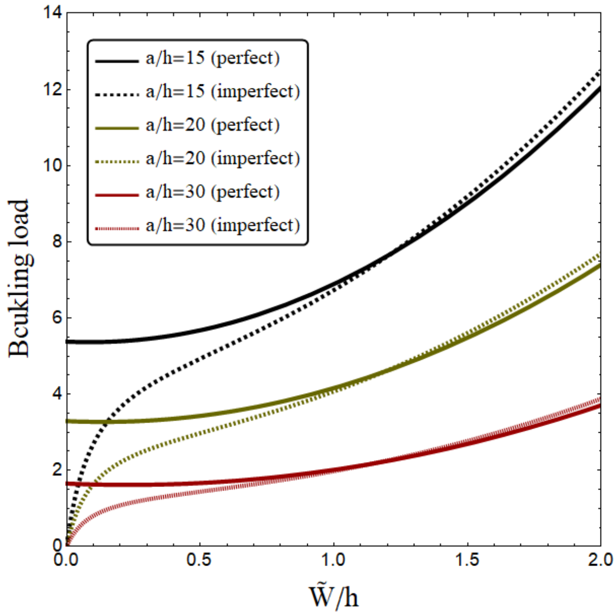

Fig. 7 Nonlinear buckling load versus normalized deflection of stiffened porous shell based on various length-to-thickness rations (R/a=4, W*/h=0.1, e_0=0.2, s_x=0.2a, h_x=0.1h, d_x=0.01a)

significant reduction in stiffness of single-curved shell in the presence of porosities inside the material structure.

In Fig. 5, the load-deflection curves have been illustrated based on the types of porosity distribution at a fixed value of porosity coefficient e_0=0.5. Obtained results show that the curved shell with non-uniform porosity distribution has higher nonlinear buckling load and pressure than uniform porosity distribution. This indicates that the curved shell with non-uniform distributed porosity can achieve the highest shell stiffness hence the best mechanical performance. Therefore, porosity distribution has a major role on the buckling behavior and should be considered in stability analysis of curved shells. As stated, the material properties of porous curved shells are constant thorough the thickness for uniform porosity distribution. While, the material properties are maximum at upper and lower surfaces for non-uniform porosity distribution.

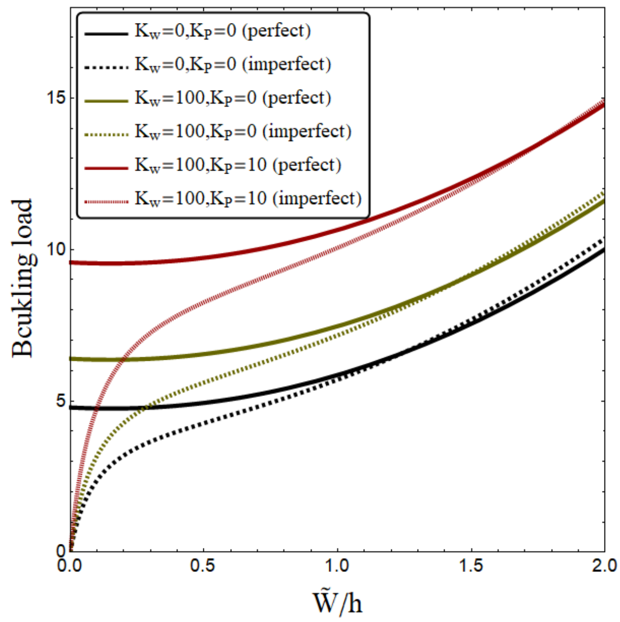

Fig. 8 Nonlinear buckling load versus normalized deflection of porous shell based on various length-to-thickness rations (a/h=15, R/a=4, s_x=0.3a, h_x=0.1h, d_x=0.01a, W*/h=0.1, e_0=0.2)

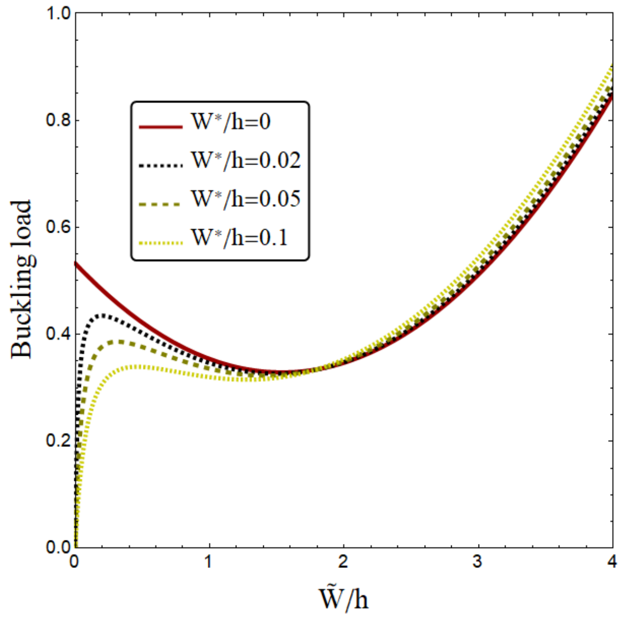

Fig. 9 Nonlinear buckling load versus normalized deflection of porous shell based on various length-to-thickness rations (a/h=50, R/a=4, e_0=0.2)

Fig. 6 indicates the post-bucking curves of the porous shell with and without the effect of stiffeners. Uniform porosity distribution with e_0=0.2 is considered. Geometrical parameters of the stiffener are selected as s_x=0.2a, h_x=0.1h, d_x=0.01a. This figure shows that stiffened curved shells have enhanced load carrying capacities since they are reinforced by a system of stiffeners. Therefore, post-buckling loads of stiffened curved shells are higher than those of curved shells without stiffeners. As stated before, porous curved shells have smaller buckling loads than perfect one. So, their buckling curves can be enhanced by using stiffeners leading to higher buckling loads.

Influence of length-to-thickness ratio (*a/h*) on post-buckling behavior of metal foam single-curved shells is presented in Fig. 7. Both geometrically ideal (perfect) and imperfect curved shells are considered. It is evident that curved shells are more flexible at larger side-to-thickness ratios. Therefore, obtained post-buckling loads become

Table 1 Validation of post-buckling loads of ideal and imperfect flat panel for different dimensionless amplitudes (a/R_x=0)

$\tilde{W}/h$	$W^*/h=0$		$W^*/h=0.1$	
	Chikh *et al.* (2016)	present	Chikh *et al.* (2016)	present
0	0.62411	0.62411	0	0
0.1	0.62627	0.62627	0.31853	0.31853
0.2	0.63274	0.63274	0.43334	0.43334
0.3	0.64354	0.64354	0.50047	0.50047

smaller with increase of side-to-thickness ratio at a fixed value of normalized amplitude ($\tilde{W}/h$). However, obtained post-buckling loads for various values of side-to-thickness ratio depend on the magnitude of normalized amplitude. For smaller side-to-thickness ratios, post-buckling load increases with a higher rate with respect to normalized amplitude than higher side-to-thickness ratios or thinner shells. This is because the curved shell is stiffer at small side-to-thickness ratios.

Fig. 8 indicates the variation of nonlinear buckling load of a metal foam single-curved shell versus dimensionless amplitude for various linear (K_W), shear (K_P) foundation parameters at e_0=0.2. It should be mentioned that the shear layer provides a continuous interaction with the curved shell, while linear layer has a discontinuous interaction with the doubly-curved shell. Accordingly, shear coefficient (K_P) has more effect on buckling loads than linear coefficient (K_W). Increasing foundation parameters yields larger nonlinear buckling loads by enhancing the bending rigidity of the curved shell.

Geometrical imperfection (W^*/h) effect on post-buckling behavior of metal foam doubly-curved shell is plotted in Fig. 11. One can see that the initial deflection of shell has a great influence on the post-buckling load-deflection curves. As stated, the critical buckling load vanishes with the consideration of initial geometrical imperfection or in the region of the small bending. Actually, in the case of perfect configuration ($W^*/h=0$), the curved shell is first critically buckled. Then, shell buckling strength reduces with the rise of dimensionless amplitude until a minimum value then it increases. But, in the case of imperfect configuration ($W^*/h \neq 0$), there is no buckling strength before the initial state of the shell. So, the buckling load is zero at the starting point for an imperfect curved shells. Finally, it can be deduced that post-buckling curves of perfect and imperfect curved shells become closer to each other at large dimensionless amplitudes.

6. Conclusions

The presented article dealt with the investigation of post-buckling behaviors of porous curved shells made from metallic foams having geometric imperfectness. The non-linear imperfect third-order shell model was proposed for modeling of single curvature porous shells. Two kinds of pore dispersal were proposed. One could see that post-buckling paths of metallic foam curved shell has dependency on the values of porosity factor, knowing that structural stiffness declines by the increase of porosity factor. Other substantial issue on post-buckling behaviors of the metallic foam curved shell was the kind of pore dispersal inside the material texture. The lowest post-buckling loads were achieved for the case of uniform pore dispersal. Taking into account geometric imperfectness, the post-buckling loads were prominently distinct from ideal metallic foam curved shells. Also, it was reported that stiffened curved shells have enhanced load carrying capacities.

Acknowledgements

The first and second authors would like to thank FPQ (Fidar project Qaem) for providing the fruitful and useful help.

References

Abdelaziz, H.H., Meziane, M. A. A., Bousahla, A. A., Tounsi, A., Mahmoud, S.R. and Alwabli, A.S. (2017), “An efficient hyperbolic shear deformation theory for bending, buckling and free vibration of FGM sandwich plates with various boundary conditions”, *Steel Compos. Struct.*, **25**(6), 693-704. https://doi.org/10.12989/scs.2017.25.6.693.

Abualnour, M., Chikh, A., Hebali, H., Kaci, A., Tounsi, A., Bousahla, A.A. and Tounsi, A. (2019), “Thermomechanical analysis of antisymmetric laminated reinforced composite plates using a new four variable trigonometric refined plate theory”, *Comput. Concrete*, **24**(6), 489-498.

Addou, F.Y., Meradjah, M., Bousahla, A.A., Benachour, A., Bourada, F., Tounsi, A. and Mahmoud, S.R. (2019), “Influences of porosity on dynamic response of FG plates resting on Winkler/Pasternak/Kerr foundation using quasi 3D HSDT. *Comput. Concrete*, **24**(4), 347-367. https://doi.org/10.12989/cac.2019.24.4.347.

Ahmed, R.A., Fenjan, R.M. and Faleh, N.M. (2019), “Analyzing post-buckling behavior of continuously graded FG nanobeams with geometrical imperfections”, *Geomech. Eng.*, **17**(2), 175-180. https://doi.org/10.12989/gae.2019.17.2.175.

Alimirzaei *et al.* (2019), “Nonlinear analysis of viscoelastic micro-composite beam with geometrical imperfection using FEM: MSGT electro-magneto-elastic bending, buckling and vibration solutions", *Struct. Eng. Mech.*, 71(5), 485-502.

Al-Maliki, A.F., Faleh, N.M. and Alasadi, A.A. (2019), "Finite element formulation and vibration of nonlocal refined metal foam beams with symmetric and non-symmetric porosities", *Struct. Monit. Maint.*, **6**(2), 147-159. https://doi.org/10.12989/smm.2019.6.2.147.

Attia, A., Bousahla, A.A., Tounsi, A., Mahmoud, S.R. and Alwabli, A.S. (2018), "A refined four variable plate theory for thermoelastic analysis of FGM plates resting on variable elastic foundations", *Struct. Eng. Mech.*, **65**(4), 453-464. https://doi.org/10.12989/sem.2018.65.4.453.

Atmane, H.A., Tounsi, A., Bernard, F .and Mahmoud, S.R. (2015), "A computational shear displacement model for vibrational analysis of functionally graded beams with porosities", *Steel Compos. Struct.*, **19**(2), 369-384. https://doi.org/10.12989/scs.2015.19.2.369.

Azimi, M., Mirjavadi, S.S., Shafiei, N. and Hamouda, A.M.S. (2017), "Thermo-mechanical vibration of rotating axially functionally graded nonlocal Timoshenko beam", *Appl. Phys. A*, **123**(1), 104. https://doi.org/10.1007/s00339-016-0712-5.

Azimi, M., Mirjavadi, S.S., Shafiei, N., Hamouda, A.M.S. and Davari, E. (2018), "Vibration of rotating functionally graded Timoshenko nano-beams with nonlinear thermal distribution", *Mech. Adv. Mater. Struct.*, **25**(6), 467-480.

Barati, M.R. and Zenkour, A.M. (2018), "Post-buckling analysis of imperfect multi-phase nanocrystalline nanobeams considering nanograins and nanopores surface effects", *Compos. Struct.*, **184**, 497-505. https://doi.org/10.1016/j.compstruct.2017.10.019.

Balubaid, M., Tounsi, A., Dakhel, B. and Mahmoud, S.R. (2019). Free vibration investigation of FG nanoscale plate using nonlocal two variables integral refined plate theory", *Comput. Concrete*, **24**(6), 579-586.

Bedia, W.A., Houari, M.S.A., Bessaim, A., Bousahla, A.A., Tounsi, A., Saeed, T. and Alhodaly, M.S. (2019), "A new hyperbolic two-unknown beam model for bending and buckling analysis of a nonlocal strain gradient nanobeams", *J. Nano Res.*, **57**, 175-191). Trans Tech Publications. https://doi.org/10.4028/www.scientific.net/JNanoR.57.175.

Belbachir, N., Draich, K., Bousahla, A.A., Bourada, M., Tounsi, A. and Mohammadimehr, M. (2019), "Bending analysis of anti-symmetric cross-ply laminated plates under nonlinear thermal and mechanical loadings", *Steel Compos. Struct.*, **33**(1), 81-92. https://doi.org/10.12989/scs.2019.33.1.081.

Bellifa, H., Bakora, A., Tounsi, A., Bousahla, A.A. and Mahmoud, S.R. (2017), "An efficient and simple four variable refined plate theory for buckling analysis of functionally graded plates", *Steel Compos. Struct.*, **25**(3), 257-270. https://doi.org/10.12989/scs.2017.25.3.257.

Berghouti, H., Adda Bedia, E.A., Benkhedda, A and Tounsi, A. (2019). Vibration analysis of nonlocal porous nanobeams made of functionally graded material", *Adv. Nano Res.*, **7**(5), 351-364. https://doi.org/10.12989/anr.2019.7.5.351.

Boukhlif, Z., Bouremana, M., Bourada, F., Bousahla, A.A., Bourada, M., Tounsi, A. and Al-Osta, M.A. (2019), "A simple quasi-3D HSDT for the dynamics analysis of FG thick plate on elastic foundation", *Steel Compos. Struct.*, **31**(5), 503-516. https://doi.org/10.12989/scs.2019.31.5.503.

Boulefrakh, L., *et al.* (2019), "The effect of parameters of visco-Pasternak foundation on the bending and vibration properties of a thick FG plate", *Geomech. Eng.*, **18**(2), 161-178. https://doi.org/10.12989/gae.2019.18.2.161.

Bourada, F., Bousahla, A.A., Bourada, M., Azzaz, A., Zinata, A. and Tounsi, A. (2019), "Dynamic investigation of porous functionally graded beam using a sinusoidal shear deformation theory", *Wind Struct.*, **28**(1), 19-30. https://doi.org/10.12989/was.2019.28.1.019.

Boutaleb, S., Benrahou, K.H., Bakora, A., Algarni, A., Bousahla, A.A., Tounsi, A. and Mahmoud, S.R. (2019), "Dynamic analysis of nanosize FG rectangular plates based on simple nonlocal quasi 3D HSDT", *Adv. Nano Res.*, 7(3), 191. https://doi.org/10.12989/anr.2019.7.3.191.

Chaabane, L.A., Bourada, F., Sekkal, M., Zerouati, S., Zaoui, F.Z., Tounsi, A. and Tounsi, A. (2019), "Analytical study of bending and free vibration responses of functionally graded beams resting on elastic foundation", *Struct. Eng. Mech.*, 71(2), 185-196. https://doi.org/10.12989/sem.2019.71.2.185.

Chen, D., Yang, J. and Kitipornchai, S. (2015), "Elastic buckling and static bending of shear deformable functionally graded porous beam", *Compos. Struct.*, **133**, 54-61. https://doi.org/10.1016/j.compstruct.2015.07.052.

Chen, D., Kitipornchai, S. and Yang, J. (2016), "Nonlinear free vibration of shear deformable sandwich beam with a functionally graded porous core", *Thin-Wall. Struct.*, **107**, 39-48. https://doi.org/10.1016/j.tws.2016.05.025.

Chikh, A., Bakora, A., Heireche, H., Houari, M.S.A., Tounsi, A. and Bedia, E.A. (2016), "Thermo-mechanical postbuckling of symmetric S-FGM plates resting on Pasternak elastic foundations using hyperbolic shear deformation theory", *Struct. Eng. Mech.*, **57**(4), 617-639. https://doi.org/10.12989/sem.2016.57.4.617.

Draiche, K., *et al.* (2019), "Static analysis of laminated reinforced composite plates using a simple first-order shear deformation theory", *Comput. Concrete*, **24**(4), 369-378. https://doi.org/10.12989/cac.2019.24.4.369.

Duc, N.D., Cong, P.H. and Quang, V.D. (2016), "Thermal stability of eccentrically stiffened FGM plate on elastic foundation based on Reddy's third-order shear deformation plate theory", *J. Therm. Stresses*, **39**(7), 772-794. https://doi.org/10.1080/01495739.2016.1188638.

Duc, N.D. and Quan, T.Q. (2014), "Transient responses of functionally graded double curved shallow shells with temperature-dependent material properties in thermal environment", *Eur. J. Mech.-A/Solids*, **47**, 101-123. https://doi.org/10.1016/j.euromechsol.2014.03.002.

Fenjan, R.M., Ahmed, R.A., Alasadi, A.A. and Faleh, N.M. (2019), "Nonlocal strain gradient thermal vibration analysis of double-coupled metal foam plate system with uniform and non-uniform porosities," *Coupled Syst. Mech.*, **8**(3), 247-257. https://doi.org/10.12989/csm.2019.8.3.247.

Hussain, M., Naeem, M.N., Tounsi, A. and Taj, M. (2019), "Nonlocal effect on the vibration of armchair and zigzag SWCNTs with bending rigidity", *Adv. Nano Res.*, **7**(6), 431. https://doi.org/10.12989/anr.2019.7.6.431.

Kaddari, B., *et al.* (2020), "A study on the structural behaviour of functionally graded porous plates on elastic foundation using a new quasi-3D model: Bending and Free vibration analysis", *Comput. Concrete*, **25**(1), 37-57. https://doi.org/10.12989/cac.2020.25.1.037.

Karami, B., *et al.* (2019), "Wave propagation of functionally graded anisotropic nanoplates resting on Winkler-Pasternak foundation", *Struct. Eng. Mech.*, **7**(1), 55-66. https://doi.org/10.12989/sem.2019.70.1.055.

Karami, B., Janghorban, M. and Tounsi, A. (2019), "On pre-stressed functionally graded anisotropic nanoshell in magnetic field", *J. Brazilian Soc. Mech. Sci. Eng.*, **41**(11), 495. https://doi.org/10.1007/s40430-019-1996-0.

Kim, S.E., Duc, N.D., Nam, V.H. and Van Sy, N. (2019), "Nonlinear vibration and dynamic buckling of eccentrically oblique stiffened FGM plates resting on elastic foundations in thermal environment", *Thin-Wall. Struct.*, **142**, 287-296. https://doi.org/10.1016/j.tws.2019.05.013.

Khiloun, M., Bousahla, A.A., Kaci, A., Bessaim, A., Tounsi, A. and Mahmoud, S.R. (2019), "Analytical modeling of bending and vibration of thick advanced composite plates using a four-variable quasi 3D HSDT", *Eng. with Comput.*, 1-15. https://doi.org/10.1007/s00366-019-00732-1.

Khosravi, F., Hosseini, S.A. and Tounsi, A. (2020), "Torsional dynamic response of viscoelastic SWCNT subjected to linear and harmonic torques with general boundary conditions via Eringen's nonlocal differential model", *Eur. Phys. J. Plus*, **135**(2), 183.

Li, H., Pang, F., Gong, Q. and Teng, Y. (2019), Free vibration analysis of axisymmetric functionally graded doubly-curved shells with un-uniform thickness distribution based on Ritz method", *Compos. Struct.*, **225**, 111145. https://doi.org/10.1016/j.compstruct.2019.111145.

Mahmoudi, A., Benyoucef, S., Tounsi, A., Benachour, A., Adda Bedia, E.A. and Mahmoud, S.R. (2019), "A refined quasi-3D shear deformation theory for thermo-mechanical behavior of functionally graded sandwich plates on elastic foundations", *J. Sandw. Struct. Mater.*, **21**(6), 1906-1929. https://doi.org/10.1177%2F1099636217727577.

Mechab, I., Mechab, B., Benaissa, S., Serier, B and Bouiadjra, B. B. (2016), "Free vibration analysis of FGM nanoplate with porosities resting on Winkler Pasternak elastic foundations based on two-variable refined plate theories", *J. Brazilian Soc. Mech. Sci. Eng.*, **38**(8), 2193-2211. https://doi.org/10.1007/s40430-015-0482-6.

Medani, M., Benahmed, A., Zidour, M., Heireche, H., Tounsi, A., Bousahla, A.A. and Mahmoud, S.R. (2019), "Static and dynamic behavior of (FG-CNT) reinforced porous sandwich plate using energy principle", *Steel Compos. Struct.*, **32**(5), 595-610. https://doi.org/10.12989/scs.2019.32.5.595.

Meksi, R., Benyoucef, S., Mahmoudi, A., Tounsi, A., Adda Bedia, E.A. and Mahmoud, S.R. (2019), "An analytical solution for bending, buckling and vibration responses of FGM sandwich plates", *J. Sandw. Struct. Mater.*, **21**(2), 727-757. https://doi.org/10.1177%2F1099636217698443.

Mirjavadi, S.S., Rabby, S., Shafiei, N., Afshari, B.M. and Kazemi, M. (2017), "On size-dependent free vibration and thermal buckling of axially functionally graded nanobeams in thermal environment", *Appl. Phys. A*, **123**(5), 315. https://doi.org/10.1007/s00339-017-0918-1.

Mirjavadi, S.S., Afshari, B.M., Shafiei, N., Hamouda, A.M.S. and Kazemi, M. (2017), "Thermal vibration of two-dimensional functionally graded (2D-FG) porous Timoshenko nanobeams", *Steel Compos. Struct.*, **25**(4), 415-426. https://doi.org/10.12989/scs.2017.25.4.415.

Mirjavadi, S.S., Afshari, B.M., Barati, M.R. and Hamouda, A.M.S. (2018), "Strain gradient based dynamic response analysis of heterogeneous cylindrical microshells with porosities under a moving load", *Mater. Res. Express*, **6**(3), 035029.

Mirjavadi, S.S., Afshari, B.M., Khezel, M., Shafiei, N., Rabby, S. and Kordnejad, M. (2018), "Nonlinear vibration and buckling of functionally graded porous nanoscaled beams", *J. Brazilian Soc. Mech. Sci. Eng.*, **40**(7), 352. https://doi.org/10.1007/s40430-018-1272-8.

Mirjavadi, S.S., Forsat, M., Hamouda, A.M.S. and Barati, M.R. (2019), "Dynamic response of functionally graded graphene nanoplatelet reinforced shells with porosity distributions under transverse dynamic loads", *Mater. Res. Express*, **6**(7), 075045.

Mirjavadi, S.S., Forsat, M., Nikookar, M., Barati, M.R. and Hamouda, A.M.S. (2019), "Nonlinear forced vibrations of sandwich smart nanobeams with two-phase piezo-magnetic face sheets", *Eur. Phys. J. Plus*, **134**(10), 508. https://doi.org/10.1140/epjp/i2019-12806-8.

Mirjavadi, S.S., Afshari, B.M., Barati, M.R. and Hamouda, A.M. S. (2019), "Transient response of porous FG nanoplates subjected to various pulse loads based on nonlocal stress-strain gradient theory", *Eur. J. Mech.-A/Solids*, **74**, 210-220. https://doi.org/10.1016/j.euromechsol.2018.11.004.

Mirjavadi, S.S., Afshari, B.M., Barati, M.R. and Hamouda, A.M.S. (2019), "Nonlinear free and forced vibrations of graphene nanoplatelet reinforced microbeams with geometrical imperfection", *Microsystem Technologies*, **25**, 3137-3150. https://doi.org/10.1007/s00542-018-4277-4.

Mirjavadi, S.S., Forsat, M., Barati, M.R., Abdella, G.M., Hamouda, A.M.S., Afshari, B.M. and Rabby, S. (2019), "Post-buckling analysis of piezo-magnetic nanobeams with geometrical imperfection and different piezoelectric contents", *Microsystem Technologies*, **25**(9), 3477-3488. https://doi.org/10.1007/s00542-018-4241-3.

Mirjavadi, S.S., Forsat, M., Barati, M.R., Abdella, G.M., Afshari, B.M., Hamouda, A.M.S. and Rabby, S. (2019), "Dynamic response of metal foam FG porous cylindrical micro-shells due to moving loads with strain gradient size-dependency", *Eur. Phys. J. Plus*, **134**(5), 214. https://doi.org/10.1140/epjp/i2019-12540-3.

Nebab, M., Atmane, H.A., Bennai, R. and Tahar, B. (2019), "Effect of nonlinear elastic foundations on dynamic behavior of FG plates using four-unknown plate theory", *Earthq. Struct.*, **17**(5), 447-462. https://doi.org/10.12989/eas.2019.17.5.447.

Quan, T.Q., Kim, S.E. and Duc, N.D. (2019), "Nonlinear dynamic response and vibration of shear deformable piezoelectric functionally graded truncated conical panel in thermal environments", *Eur. J. Mech.-A/Solids*, **77**, 103795. https://doi.org/10.1016/j.euromechsol.2019.103795.

Sahla, M., Saidi, H., Draiche, K., Bousahla, A.A., Bourada, F. and Tounsi, A. (2019), "Free vibration analysis of angle-ply laminated composite and soft core sandwich plates", *Steel Compos. Struct.*, **33**(5), 663. https://doi.org/10.12989/scs.2019.33.5.663.

Tlidji, Y., *et al.* (2019), "Vibration analysis of different material distributions of functionally graded microbeam", *Struct. Eng. Mech.*, **69**(6), 637-649. https://doi.org/10.12989/sem.2019.69.6.637.

Trinh, M.C., Nguyen, D.D. and Kim, S.E. (2019), "Effects of porosity and thermomechanical loading on free vibration and nonlinear dynamic response of functionally graded sandwich shells with double curvature", *Aerosp. Sci. Techno.*, **87**, 119-132. https://doi.org/10.1016/j.ast.2019.02.010.

Trinh, M.C. and Kim, S.E. (2018), "Nonlinear thermomechanical behaviors of thin functionally graded sandwich shells with double curvature", *Compos. Struct.*, **195**, 335-348. https://doi.org/10.1016/j.compstruct.2018.04.067.

Trinh, M.C. and Kim, S.E. (2019a), "Nonlinear stability of moderately thick functionally graded sandwich shells with double curvature in thermal environment", *Aerosp. Sci. Technol.*, **84**, 672-685. https://doi.org/10.1016/j.ast.2018.09.018.

Trinh, M.C. and Kim, S.E. (2019b), "A three variable refined shear deformation theory for porous functionally graded doubly curved shell analysis", *Aerosp. Sci. Technol.*, **94**, 105356. https://doi.org/10.1016/j.ast.2019.105356.

Wattanasakulpong, N and Ungbhakorn, V. (2014), "Linear and nonlinear vibration analysis of elastically restrained ends FGM beams with porosities", *Aerosp. Sci. Technol.*, **32**(1), 111-120. https://doi.org/10.1016/j.ast.2013.12.002.

Zare Jouneghani, F., Dimitri, R., Bacciocchi, M. and Tornabene, F. (2017), "Free vibration analysis of functionally graded porous doubly-curved shells based on the first-order shear deformation theory", *Appl. Sci.*, **7**(12), 1252. https://doi.org/10.3390/app7121252.

Zarga, D., Tounsi, A., Bousahla, A.A., Bourada, F. and Mahmoud, S.R. (2019), "Thermomechanical bending study for functionally graded sandwich plates using a simple quasi-3D shear deformation theory", *Steel Compos. Struct.*, **32**(3), 389-410. https://doi.org/10.12989/scs.2019.32.3.389.

Zaoui, F.Z., *et al.* (2019), "New 2D and quasi-3D shear deformation theories for free vibration of functionally graded plates on elastic foundations", *Compos. Part B*, **159**, 231-247. https://doi.org/10.1016/j.compositesb.2018.09.051.

Zhao, J., Xie, F., Wang, A., Shuai, C., Tang, J. and Wang, Q. (2019), "A unified solution for the vibration analysis of functionally graded porous (FGP) shallow shells with general boundary conditions", *Compos. Part B: Eng.*, **156**, 406-424. https://doi.org/10.1016/j.compositesb.2018.08.115.

Zine, A., Tounsi, A., Draiche, K., Sekkal, M. and Mahmoud, S.R. (2018), "A novel higher-order shear deformation theory for bending and free vibration analysis of isotropic and multilayered plates and shells", *Steel Compos. Struct.*, **26**(2), 125-137. https://doi.org/10.12989/scs.2018.26.2.125.

CC